



HAL
open science

3D Ruthenium Nanoparticle Covalent Assemblies from Polymantane Ligands for Confined Catalysis

Yuanyuan Min, Houssein Nasrallah, Didier Poinso, Pierre Lecante, Yann Tison, Hervé Martinez, Pierre Roblin, Andrea Falqui, Romuald Poteau, Iker Del ros, et al.

► **To cite this version:**

Yuanyuan Min, Houssein Nasrallah, Didier Poinso, Pierre Lecante, Yann Tison, et al.. 3D Ruthenium Nanoparticle Covalent Assemblies from Polymantane Ligands for Confined Catalysis. *Chemistry of Materials*, 2020, 32 (6), pp.2365-2378. 10.1021/acs.chemmater.9b04737 . hal-02541912

HAL Id: hal-02541912

<https://hal.science/hal-02541912>

Submitted on 19 Oct 2020

HAL is a multi-disciplinary open access archive for the deposit and dissemination of scientific research documents, whether they are published or not. The documents may come from teaching and research institutions in France or abroad, or from public or private research centers.

L'archive ouverte pluridisciplinaire **HAL**, est destinée au dépôt et à la diffusion de documents scientifiques de niveau recherche, publiés ou non, émanant des établissements d'enseignement et de recherche français ou étrangers, des laboratoires publics ou privés.



Open Archive Toulouse Archive Ouverte (OATAO)

OATAO is an open access repository that collects the work of Toulouse researchers and makes it freely available over the web where possible

This is a Publisher's version published in: <http://oatao.univ-toulouse.fr/26115>

Official URL: <https://doi.org/10.1021/acs.chemmater.9b04737>

To cite this version:

Min, Yuanyuan  and Nasrallah, Houssein and Poinso, Didier and Lecante, Pierre and Tison, Yann and Martinez, Hervé and Roblin, Pierre  and Falqui, Andrea and Poteau, Romuald and del Rosal, Iker and Gerber, Iann C. and Hierso, Jean-Cyrille and Axet Marti, Maria Rosa  and Serp, Philippe  *3D Ruthenium Nanoparticle Covalent Assemblies from Polymantane Ligands for Confined Catalysis*. (2020) *Chemistry of Materials*, 32 (6). 2365-2378. ISSN 0897-4756

Any correspondence concerning this service should be sent to the repository administrator: tech-oatao@listes-diff.inp-toulouse.fr

3D Ruthenium Nanoparticle Covalent Assemblies from Polymantane Ligands for Confined Catalysis

Yuanyuan Min, Houssein Nasrallah, Didier Poinsot, Pierre Lecante, Yann Tison, Hervé Martinez, Pierre Roblin, Andrea Falqui, Romuald Poteau, Iker del Rosal, Iann C. Gerber, Jean-Cyrille Hierso, M. Rosa Axet, and Philippe Serp

Chem. Mater., **Just Accepted Manuscript** • DOI: 10.1021/acs.chemmater.9b04737 • Publication Date (Web): 19 Feb 2020

Just Accepted

“Just Accepted” manuscripts have been peer-reviewed and accepted for publication. They are posted online prior to technical editing, formatting for publication and author proofing. The American Chemical Society provides “Just Accepted” as a service to the research community to expedite the dissemination of scientific material as soon as possible after acceptance. “Just Accepted” manuscripts appear in full in PDF format accompanied by an HTML abstract. “Just Accepted” manuscripts have been fully peer reviewed, but should not be considered the official version of record. They are citable by the Digital Object Identifier (DOI®). “Just Accepted” is an optional service offered to authors. Therefore, the “Just Accepted” Web site may not include all articles that will be published in the journal. After a manuscript is technically edited and formatted, it will be removed from the “Just Accepted” Web site and published as an ASAP article. Note that technical editing may introduce minor changes to the manuscript text and/or graphics which could affect content, and all legal disclaimers and ethical guidelines that apply to the journal pertain. ACS cannot be held responsible for errors or consequences arising from the use of information contained in these “Just Accepted” manuscripts.

3D Ruthenium Nanoparticle Covalent Assemblies from Polymantane Ligands for Confined Catalysis

Yuanyuan Min,[†] Houssein Nasrallah[‡] Didier Poinso[‡] Pierre Lecante,[§] Yann Tison,^{||} Hervé Martinez,^{||} Pierre Roblin,[#] Andrea Falqui,^{*} Romuald Poteau,[¶] Iker del Rosal,[¶] Iann C. Gerber,^{*,¶} Jean-Cyrille Hierso,^{*,‡} M. Rosa Axet^{*,†} and Philippe Serp^{*,†}.

[†] LCC-CNRS, INPT, 205 route de Narbonne, 31077 Toulouse Cedex 4, France

[‡] Institut de Chimie Moléculaire de l'Université de Bourgogne (ICMUB - UMR CNRS 6302), Université de Bourgogne Franche-Comté (UBFC), 9 avenue Alain Savary, 21078 Dijon Cedex, France

[§] Centre d'élaboration des matériaux et d'études structurales UPR CNRS 8011, 29 Rue Jeanne-Marvig, BP 4347, 31055 Toulouse, France

^{||} Université de Pau et des Pays de l'Adour, e2s UPPA, IPREM CNRS UMR 5254, 2 Avenue du président Angot, Pau, 64053, France.

[#] Laboratoire de Génie Chimique and Fédération de Recherche FERMAT, 4 allée Emile Monso, 31030 Toulouse, France

^{*} King Abdullah University of Science and Technology (KAUST), Biological and Environmental Sciences and Engineering (BESE) Division, NABLA Lab, 23955 Thuwal, Saudi Arabia

[¶] INSA-CNRS-UPS, LPCNO, Université Fédérale de Toulouse Midi-Pyrénées, 135 Avenue de Rangueil, F-31077 Toulouse, France

ABSTRACT: The synthesis of metal nanoparticle (NP) assemblies stabilized by functional molecules is an important research topic in nanoscience, and the ability to control interparticle distances and positions in NP assemblies is one of the major challenges in designing and understanding functional nanostructures. Here, two series of functionalized adamantanes, bis-adamantanes and diamantanes bearing carboxylic acid or amine functional groups have been used as building blocks to produce, *via* a straightforward method, networks of ruthenium NP. Both the nature of the ligand and the Ru/ligand ratio affect the interparticle distance in the assemblies. The use of 1,3-adamantanedicarboxylic acid allows the synthesis of 3D networks of 1.7-1.9 nm Ru NP presenting interparticle distance of 2.5-2.7 nm. The surface interaction between Ru NP and the ligands were investigated spectroscopically using a ¹³C labeled ligand, as well as theoretically with Density Functional Theory (DFT) calculations. We found that Ru species formed during the NP assembly are able to partially decarbonylate carboxylic acid ligands at room temperature. Decarbonylation of a carboxylic acid at room temperature in the presence of dihydrogen usually occurs on catalysts at much higher temperature and pressure. This result reveals a very high reactivity of ruthenium species formed during network assembling. The Ru NP networks were found active catalysts for the selective hydrogenation of phenyl acetylene, reaching good selectivity towards styrene. Overall, we demonstrated that catalyst activity, selectivity, and NP network stability are significantly affected by Ru NP interparticle distance, and electronic ligand effects. As such, these materials constitute a unique set that should allow a better understanding of the complex surface chemistry in carbon-supported metal catalysts.

INTRODUCTION

The self-assembly of molecules, clusters or nanostructures is a promising avenue for the development of organized nanostructures with peculiar properties and broad spectrum of emerging applications.¹⁻⁴ In the case of metallic nanoparticles (NP), a combination of self- and directed

assembly processes involving interparticle forces can be used to produce the desired materials.⁴ These processes generally involve non-covalent interactions between NP,⁴ resulting in assemblies of poor stability, which can be detrimental for some applications. To obtain stable NP assemblies, molecular mediators that can induce a covalent bond between the NP have to be used. Such molecules

enable interparticle distance and interaction tuning in the assemblies, allowing studying not only the properties of the individual NP, but also the collective effects of the two-dimensional (2D) and three-dimensional (3D) networks of NP.⁵⁻⁷ Networks of gold⁸⁻¹⁰ and ruthenium¹¹ NP have already been described; these networks are assembled by means of di- or polytopic ligands. For instance, thiol-amine¹² and disulfide employed as ligands^{8,9} lead to 2D assemblies of Au NP, which are organized in a hexagonal array. In general, the interparticle distance can be modulated by changing the length of the alkyl chain of the ligands, and in that context, ligand rigidity should be considered. The use of multicarboxylate ligands, such as the C₆₆(COOH)₁₂ hexa-adduct, allowed producing 3D networks of Ru NP (1.6 nm) showing an interparticle distance of 2.85 nm.¹¹

For applications in catalysis, such networks of metal NP - provided they are sufficiently robust¹³ - could combine several advantages compared to traditional catalysts, such as: i) a narrow particle size distribution, ii) a controlled interparticle distance, iii) a well-defined chemical environment, and iii) the possibility to take advantage of confinement effects if porous. Whenever built from organic ligands, NP networks constitute ideal model catalysts to study carbon-supported metal catalysts and their intricate surface chemistry.^{14, 15} Indeed, such catalysts generally consist in metal NP deposited on *sp*²/*sp*³ hybridized carbon materials presenting surface functional groups that contain heteroatoms such as oxygen or nitrogen.¹⁵⁻¹⁷ Although the nature of the interaction between surface functional groups and metal NP has been identified as essential for catalysis, since it can affect both metal dispersion and metal-support interaction, it is not yet well understood.¹⁷ Thus, in the case of oxygen- and nitrogen-functionalized carbon nanotubes (CNT), it has been shown that: i) Pd NP supported on N-CNT showed a narrower size distribution than those on O-CNT; and ii) Pd/N-CNT catalyst showed better catalytic performances in selective olefin hydrogenation in terms of activity and selectivity compared to the Pd/O-CNT catalyst.¹⁸ Additionally, in such catalysts, the control of fundamental characteristics for catalysis such as particle size, interparticle distance and metal-support interaction is not achieved.

In this context, we have used bi-functional polymantanes (*i.e.* rigid *sp*³-hybridized diamondoids) as ligands to build, *via* a straightforward and up-scalable method, Ru NP networks presenting uniform particle size and interparticle distance, as well as a well-defined chemical environment. Commercially available adamantane and diamantane have mechanically rigid and thermodynamically extremely stable structures,^{19, 20} which are easily amenable to synthetic modifications,²¹⁻²³ and have been used with success to assemble various innovative functional materials.²⁴⁻²⁶ Thus, we employed adamantane, bis-adamantane and diamantane as platform for synthesizing dicarboxylic and diamine ligands, which are used for the first time to produce a set of Ru NP networks with well-defined characteristics (NP size,

interparticle distance, electronic environment) of interests for catalysis. These materials were investigated for the selective hydrogenation of phenylacetylene into styrene. The nature of the metal-ligand interface that mimics surface oxygen or nitrogen groups is shown to affect catalyst activity, selectivity but also NP network stability. A significant increase in TOF by decreasing interparticle distance is also observed.

MATERIALS AND METHODS

The solvents we used in this work were purified with a MBraun SPS-800 solvent purification system and degassed by freezing cycles. [Ru(COD)(COT)] [(1,5-cyclooctadiene)(1,3,5-cyclooctatriene)ruthenium] was purchased from Nanomeps Toulouse. 1-Adamantanecarboxylic acid (AdCOOH, **1**) and 1-Adamantylamine (AdNH₂, **5**), phenylacetylene and decane were purchased from Sigma-Aldrich and used as received. The synthesis of the other polymantanes ligands is given in the Supporting Information.

Synthesis of Ru nanoparticles. In a typical experiment [Ru(COD)(COT)] complex and the desired ligand were introduced in a Fisher-Porter bottle, solubilized with THF, and stirred 1h under argon. The resulting solution was pressurized with 3 bar of H₂. The solution, which turned black after few minutes of reaction, was kept under stirring overnight at room temperature. After this period of time, excess of H₂ was eliminated and the volume of solvent was reduced under vacuum. Pentane was then added to the colloidal suspension to precipitate the Ru nanoparticles. After filtration under argon with a cannula, the black solid powder was washed twice with pentane and filtrated again before drying under vacuum. For each ratio studied, the quantities of reactants and the obtained yields are detailed in the Supporting Information.

Synthesis of Ru complexes. The synthesis and characterizations of [Ru(adamantane carboxylate)(η^4 -1,5-COD)(η^3 -1,2,3-COD)] - **Ru₁**, [Ru₂(adamantane dicarboxylate)(η^4 -1,5-COD)₂(η^3 -1,2,3-COD)₂] - **Ru₂**, and [Ru₂(μ -adamantane carboxylate)₂(μ - η^3 - η^2 -1,2,3-COD)(η^3 -1,2,3-COD)(THF)] - **Ru₃** is given in the Supporting Information.

Synthesis of Ru NP on functionalized carbon nanotubes. 9.6 mg [Ru(COD)(COT)] dissolved in 20mL THF, was added to 150 mg of dried functionalized carbon nanotubes (O-CNT or N-CNT). After stirred under Ar atmosphere overnight, the resulted mixture was filtered and washed with pentane to obtain a black solid, which was reduced under H₂/Ar gas flow (flow ratio of Ar:H₂= 4:1) at 200 °C for 1h. The rate of increasing temperature is 7 °C/min. The final products were kept in inert atmosphere for further catalysis. ICP analyses have shown a Ru loading of 1.6% w/w for Ru/O-CNT and 0.8% for Ru/N-CNT.

Catalytic hydrogenation of phenylacetylene. In a typical catalytic reaction, a mixture of phenylacetylene (4 mmol, 412 mg), decane (0.5 mmol, 71 mg) and Ru NP catalyst (Ru atom amount 0.02 mmol) were dispersed in MeOH (25 mL) in a magnetically stirred autoclave with Teflon inner cylinder. The autoclave was purged three times with H₂. The autoclave was pressurized with 5 bar of H₂ at room temperature and stirred at 1500 rpm. Under such conditions, external mass transfer limitation should not be relevant (see ESI, S1). The suspension was continuously stirred until the end of the reaction. Gas chromatography (GC) was used to identify the products. After catalysis, samples were taken for TEM analyses, also, the % of Ru on the filtered catalytic solution was ascertained by ICP. The TOF were calculated according to the total surface Ru content (see ESI, S1).

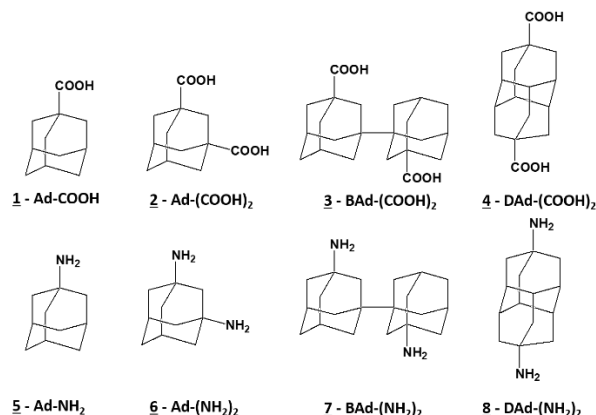
Characterization. The details of ICP, TEM, NMR, XRD, infrared, WAXS, XPS and SAXS characterization are given in the Supporting Information.

Computational details. The DFT calculations were performed using the Vienna *ab initio* simulation package VASP,²⁷⁻³⁰ based on the full-potential projector augmented wave framework,^{31,32} Exchange-correlation effects have been approximated using the spin-polarized version of PBE functional.³³ A kinetic-energy cutoff of 400 eV was found to be sufficient to achieve a total-energy convergence within several meV, considering the k-point sampling in Gamma-point only calculations for isolated molecules and complexes, in conjunction with a Gaussian smearing with a width of 0.05 eV. During geometry optimization runs, all the atoms were fully relaxed until forces on individual atoms were smaller than 0.01 eV/Å. Calculation cells for isolated molecules and complexes were (25x26x27) Å³, to avoid spurious interactions between periodic images. Figures of the different geometries were produced thanks to the 3D visualization program VESTA.³⁴ Bader charge analyses were performed using Henkelmann's group code.³⁵ The optimal geometries upon H₂ adsorption were constructed following the results of Ref.,³⁶ *i. e.* all available μ₃ sites were occupied and then the top sites and, if needed, some bridge sites were used to build the starting geometries. Reaction barriers were estimated by the climbing image nudged elastic band (CI-NEB) method³⁷⁻³⁹ with a spring force between images of 5 eV/Å² and a force tolerance of 0.05 eV/Å. The harmonic vibrational modes were systematically calculated to distinguish minima and saddle points using dynamical matrix extraction scheme of VTST tools.

RESULTS

Synthesis and characterization of Ru NP. We have used a set of carboxylic acid and amine ligands bearing the sp³-C hybridized platforms adamantane (Ad), bis-adamantane (BAd), and diamantane (DAd) (Scheme 1). 1,3-diaminoadamantane (**6**), Ad-(NH₂)₂, was prepared from 1,3-dibromoadamantane (28% yield) following a reported method.⁴⁰ The related compound BAd-(NH₂)₂, **7** was

obtained from BAd, which was itself prepared from 1-bromoadamantane homocoupling by metallic sodium.^{40, 41} From commercial diamantane, DAd-(NH₂)₂, **8** was obtained after selective dibromination of 4,9-C-H apical positions.⁴² Ad-COOH **1** and Ad-(COOH)₂, **2** are commercially available, and DAd-(COOH)₂, **4** was prepared based on literature methods and isolated (23% yield) starting from 4,9-dihydroxy-diamantane.^{43, 44} BAd-(COOH)₂, **3**, was also synthesized (see SI); however, its insolubility in common organic solvents obviated its use as stabilizer of Ru NP.



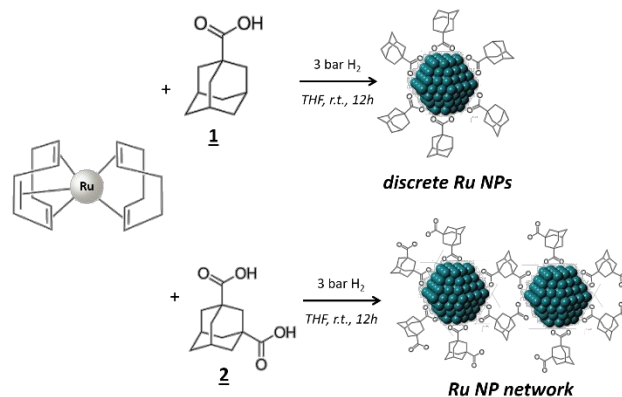
Scheme 1. Polyadamantane ligands based on adamantane, bis-adamantane, and diamantane backbone used for the stabilization of discrete Ru NPs and/or networks.

The discrete NP and NP networks reported herein were conveniently obtained by reaction of (1,5-cyclooctadiene)(1,3,5-cyclooctatriene)ruthenium(0), [Ru(COD)(COT)], at room temperature in THF under 3 bar of H₂ in the presence of the corresponding stabilizing polyadamantane ligand (see Scheme 2 for a representative example with ligands **1** and **2**).

Different amounts of ligand were employed for the synthesis of some of the Ru NP, specifically 0.2, 0.1 and 0.05 molar equiv., with the aim to obtain different sizes of nanoparticles and as such a lever to control reactivity. The size of ruthenium NP was determined by Transmission Electron Microscopy (TEM) and correlated with Wide-Angle X-ray Scattering (WAXS). In Ru NP network samples, the interparticle distances were measured by Small Angle X-ray Scattering (SAXS). The results of these analyses, as well as the Ru metal content, are reported on Table 1. Adamantane carboxylic acid **1** has already been used to stabilize FeCo₃ NP⁴⁵ and CdSe quantum dots.⁴⁶

To the best of our knowledge, the adamantane amine **5** has not been used before as ligand for surface stabilization in NP synthesis. The decomposition of [Ru(COD)(COT)] in the presence of **1** or **5** (Ru/ligand molar ratio = 10) leads to the formation of isolated Ru NP with size of 1.8 and 1.6 nm

(TEM), respectively (see Table 1 and Figure 1). Similar NP sizes were reported for Ru NP prepared from [Ru(COD)(COT)] and amines,⁴⁷ and carboxylic acid ligands.⁴⁸ The coherence length (2.2 nm, Ru NP produced from **1**) indicated by the Radial Distribution Function (RDF) resultant from WAXS analyses (Figure S1) is slightly longer than the mean diameter determined by TEM observation. This feature, which was common to many of the samples prepared (see Table 1), was already reported for ligand stabilized metal NP.⁴⁹ For amine ligands, for which a facile reversible binding leads to dynamic exchanges between free and coordinated species, Ru NP coalescence has been reported.⁵⁰ Consistently, the NP produced from the amine ligand **5** are much more agglomerated than the ones produced from the carboxylic acid ligand **1**. Adsorption energy of $-60 \text{ kcal mol}^{-1}$ was obtained for **1** on a bare Ru_{13} cluster, presenting a *syn-syn* bridging coordination with two Ru–O distances of 2.0 and 2.1 Å after the spontaneous O–H bond dissociation on the cluster, see Figure S2.



Scheme 2. Synthesis of ruthenium NP and NP networks using polymantane ligands as stabilizers.

Table 1. Mean size distributions, interparticle distances and ruthenium content of the synthesised Ru NP and Ru NP networks.

Ligand	Ru/L (molar)	Ru loading (%)	Ru NP size (nm) ^a	Ru NP size (nm) ^b	Interparticle distance (nm) ^c
1	5/1	77.9	1.5 ± 0.6	1.5	-
	10/1	65.5	1.8 ± 0.5	2.2	-
	20/1	78.7	1.9 ± 0.6	2.5	-
2	5/1	50.2	1.7 ± 0.7	1.7	2.2
	10/1	61.8	1.8 ± 0.8	2.0	2.7
4	20/1	70.1	1.9 ± 0.7	2.2	2.7
	10/1	67.7	1.8 ± 0.6	2.1	2.9
5	10/1	82.5	1.6 ± 0.7	1.5	-
6	10/1	80.1	1.8 ± 0.7	1.9	2.4
7	10/1	65.7	1.7 ± 0.6	1.2	2.5
8	10/1	70.2	1.7 ± 0.7	2.1	2.7

^a From TEM. ^b From WAXS. ^c From SAXS.

Similar energies have been obtained in a previous work involving the coordination of acetic acid on Ru_{55} .⁵¹ A significant charge transfer from the cluster to the ligand ($-0.84 e^-$, as a result of the oxygen lone pair sigma donation and π^* backdonation), with $0.27 e^-$ given to the hydride) has been estimated by Bader charge analysis. Slightly smaller adsorption energy on a bare Ru_{55} NP was calculated: $-48 \text{ kcal mol}^{-1}$, with very similar charge transfer. In the case of **5**, in agreement with previous results involving the coordination of amines on RuNP,⁵² the adsorption energy is reduced to -30 kcal/mol . This difference can be associated to a top coordination, with a single Ru–N bond-length of 2.2 Å. In the same way, a lower charge transfer ($0.12 e^-$) from the ligand to the metal is calculated. From these fundamental data, it can be anticipated that these two types of ligands (carboxylic acid vs amine) should induce different surface states for Ru NP of similar size, and possibly also different

network assembly, and as a consequence, different catalytic performances.

As expected, the use of both the bis-carboxylic acid (**2-4**) and bis-amino (**6-8**) derived bi-functional polymantanes induces the formation of networks of Ru NP (Figure 1). In these networks, the mean Ru NP size is relatively homogeneous (1.7–1.9 nm from TEM). Pleasingly, this synthetic method allows for the production of networks of metal NP with a narrow particle size distribution compared to conventional catalytic materials prepared on carbon support. Whatever the ligand used, we did not find any correlation between the amounts of adsorbed ligand (Table S1) and the Ru NP size for the isolated NP or the NP networks.

SAXS analyses were performed to evaluate the interparticle distances in the assemblies. The scattering intensity profiles (Figure 2a for ligand **2**, and Figure S3 for the other samples) show a general increase of the scattering intensity towards

small q values, which is coherent with a system constituted of Ru NP.^{11, 53} At higher values of q ($q_{max} = 0.2-0.3 \text{ \AA}^{-1}$) we observed a peak interpreted as a correlation distance between the metallic NP (center-to-center distance between Ru NP in the superstructure).^{11, 54} It is worth mentioning that SAWS analyses do not allow calculating the distance distribution. These correlation distances were found to vary between 2.2 and 2.9 nm, according to the nature of the ligand, and the Ru/L molar ratio. Slightly larger correlation distances were measured in the case of dicarboxylic ligands compared to diamine ones displaying the same backbone. This is consistent with the dimensions of these stabilizing species. The self-assembly process can be directed to tune the interparticle spacing by using BAd and DAd ligands; and with ligands **4**, **7** and **8**, larger correlation distances were measured compared to ligands **2** and **6**, respectively.

For a given ligand, the increase of the Ru/L molar ratio contributes to enhance the spatial distribution of the NP, creating a more homogeneous particle network. Indeed, for ligand **2** the SAXS curves shows at intermediate angles a correlation peak larger for the Ru/L ratio 5/1 (Figure 2a), reflecting a change in distribution of interparticle distance with an increase of the polydispersity.

In the case of ligands **2** and **6**, DFT calculations have confirmed larger interactions of the carboxylate groups compared to the diamine ones with both Ru₁₃ and Ru₅₅ NP models. With a single ligand **2**, Ru-O interactions are strong enough to avoid the coalescence of two Ru₁₃ or Ru₅₅ clusters. For ligands **6**, larger clusters are obtained due to coalescence upon geometry optimizations. See Figure 2b for the coordination mode of ligand **2** bridging two Ru₅₅ clusters. In this case, the Ru NP-Ru NP distance is 1.8 nm, measured from both NP centers.

To confirm the short-range order between the Ru NP, we performed an electron tomography (ET) analysis on a typical aggregate obtained from ligand **2** at a Ru/L molar ratio of 10 (Figure 2c). After performing ET on large NP assemblies, it was possible to determine the distribution of their distance (Figure S4) and to reconstruct the 3D shape of some of them, indicating a Ru NP mean size of 1.9 ± 0.3 nm and an interparticle distance of 2.65 nm. We have correlated these results to a higher binding energy (calculated by DFT, see Electronic Supporting Information for computational details) of **1** compared to **5** to the Ru NP. The Ru NP mean size determined by ET for this sample is in agreement with the distances evaluated by TEM and WAXS data (Table 1), and the interparticle distance is consistent with the one determined by SAXS analysis (Table 1, 2.7 nm).

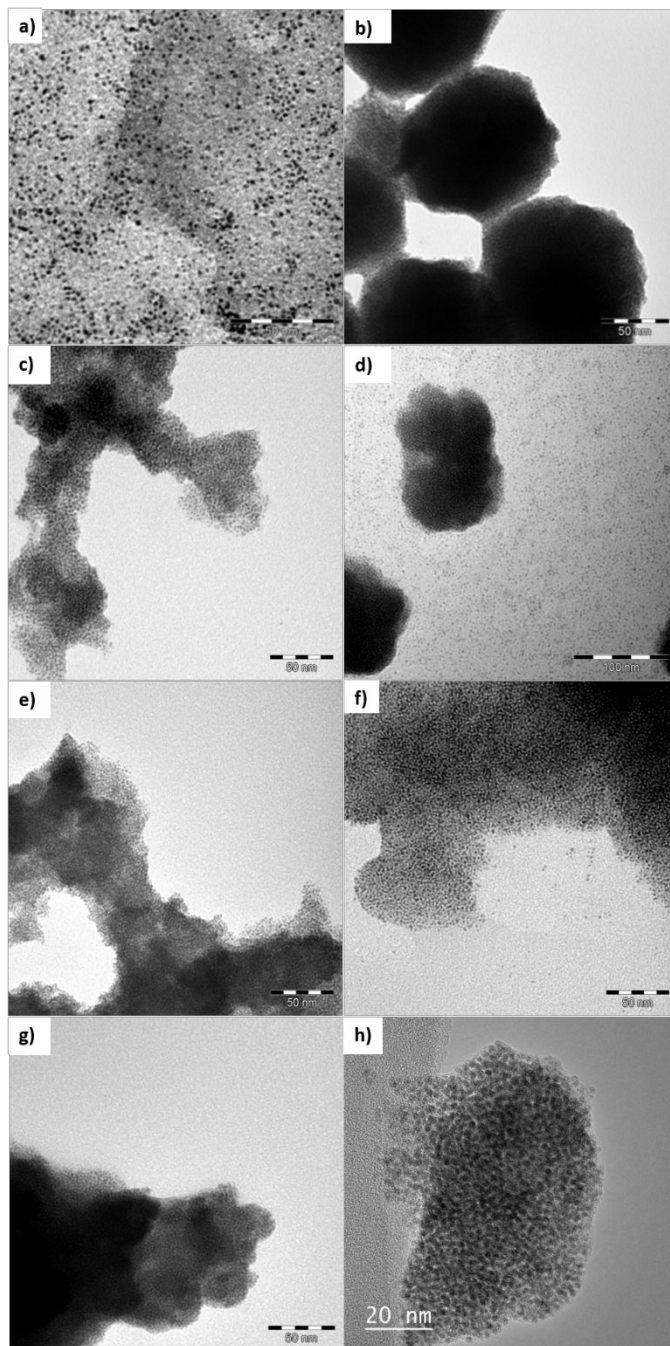


Figure 1. TEM micrographs of Ru NP and NP networks obtained at a Ru/L molar ratio of 10 for ligands: a) **1** (scale bar = 50 nm); b) **2** (scale bar = 50 nm); c) **4** (scale bar = 50 nm); d) **5** (scale bar = 100 nm); e) **6** (scale bar = 50 nm); f) **7** (scale bar = 50 nm); g) **8** (scale bar = 50 nm); and h) HRTEM of Ru@**2** (scale bar = 20 nm).

We have shown by DFT that the use of ligands **1** and **5** leads to different charge transfer between the ligand and the Ru NP. We have also investigated possible charge transfer in the case of the ligands Ad-(COOH)₂, **2**, and Ad-(NH₂)₂, **6**. DFT calculations, XPS and IR analyses show a similar tendency: the charge transfer is from the ligand to the metal with the

amine ligand, and from the metal to the ligand with the carboxylic ligand. For instance, when a single ligand **2** is bridging two Ru₅₅ NP, the charge transfer corresponds to a loss of around 0.8 e⁻ for each NP. We used carbon monoxide adsorption on the Ru NP produced from ligands **2** (**Ru@2**) and **6** (**Ru@6**) to probe the charge transfer by infrared spectroscopy.

Prior to CO adsorption, the Ru NP were first outgassed under vacuum to eliminate the CO ligands arising from the decomposition reaction (*vide infra*). After CO adsorption at room temperature, the ν_{CO} stretching frequency were measured at 2050-1940 and 1980-1920 cm⁻¹ for **Ru@2** and **Ru@6**, respectively (see Figure S5 for the corresponding spectra). The use of the donor ligand **6**, contributes to increase the electronic density on Ru NP, and consequently to a significant Ru → CO π-donation.

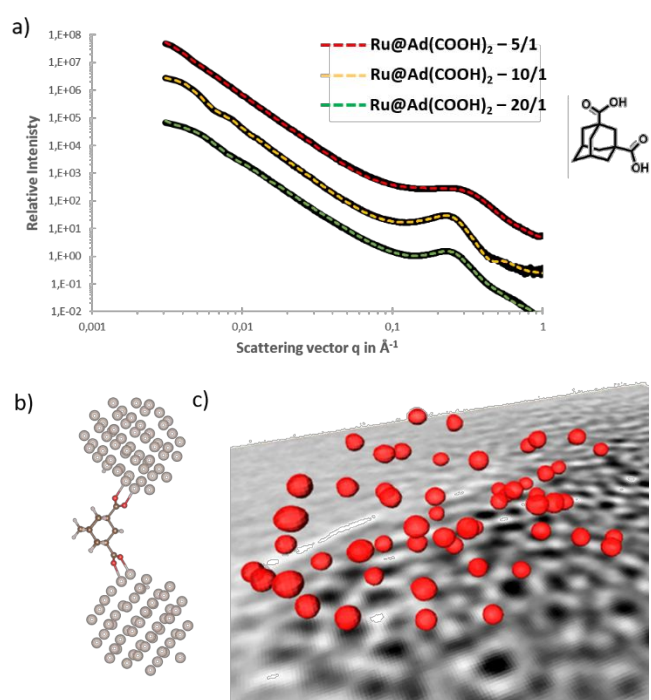


Figure 2. a) SAXS patterns of Ru NP assembly produced from ligand **2** at different Ru/L molar ratio 5/1, 10/1 and 20/1. The experimental SAXS curves are plotted in Log I(q) fct Log q representation in black line and the fitting curves corresponding to the computed SAXS curves from model are plotted in red line for the Ru/L molar ratio 5/1, in yellow for the molar ratio 10/1 and in green for the molar ratio 20/1. For the plot molar ratio 5/1, the contributions of the different components of the model (surface description, elementary object and distance between particle), are shown in dashed line with the principal corresponding fitting parameters. The sum of these three contributions gives the red fitting curve. b) Optimized structure of the (Ru₅₅)₂@Ad-(COO)₂ species; and c) 3D manual reconstruction of some Ru NP from the corresponding tomogram. A slice of the latter was used just as a visual background for the NP. It should be noticed that not all the NP imaged by ET are reported, but just few of them, properly chosen in order to make it clearly distinguishable. Their size is calculated to be 1.9 ± 0.3 nm.

The increase of the electronic density in the CO π* causes the C–O bond length to increase and thus the ν_{CO} to decrease. In the case of ligand **2**, the charge transfer occurs from the metal to the ligand, and consequently the ν_{CO} shifted to higher wavenumber. XPS analyses support the charge repartition deduced from DFT/IR. The details of the analyses of **Ru@2** and **Ru@6** at a Ru/L molar ratio of 10 are given in Tables S2 and S3 and Figure S6. As far as the Ru (3d) and (3p) core levels are concerned, the data obtained for the Ru 3d_{5/2}, Ru 3d_{3/2} and Ru 3p_{3/2} peaks are consistent with metallic Ru.⁵⁵ A slight difference in the binding energy of the Ru 3p_{3/2} peaks between the product obtained from ligands **2** (461.3 eV) and **6** (461.2 eV) is consistent with Ru NP that are more electro-deficient in the case of ligand **2**.

Surface coordination chemistry. The coordination of primary amine⁵⁶ and carboxylic acid ligands⁴⁹ to Ru NP

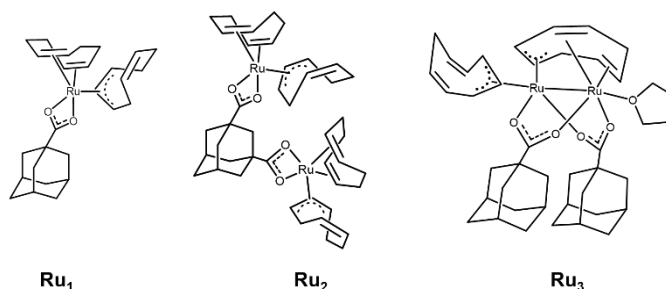
prepared by the decomposition of [Ru(COD)(COT)] has been studied: NMR contributed to demonstrate the coordination of octylamine to the surface of Ru NP.⁵⁷ Herein, the coordination of **6** by the amine has been confirmed experimentally by XPS, IR and SS-NMR. In XPS, the N 1s spectrum of **Ru@6** shows a peak at 398.6 eV (see Table S3 and Figure S6), which corresponds to a surface-attached nitrogen atom transferring electron density to the Ru surface *via* its lone pair. Consistently, it was also reported that the coordination of primary amines such as hexadecylamine to iron oxide NP gives a binding energy (BE) at 399.7 eV, whereas the corresponding free amine gives a BE value at 397.2 eV.⁵⁷ Figure S7 shows the IR and SS-NMR spectra of the free ligand **6** and of **Ru@6**. The IR spectrum of **Ru@6** shows bands at 3275-3205 and 2903-2852 cm⁻¹ corresponding to the N–H and C–H stretching bands of

the ligand, respectively; confirming the presence of amine ligands near the surface of the particles. The ^{13}C SS-NMR spectrum of **Ru@6** shows broad bands at 30–50 ppm characteristic of the sp^3 carbons of ligand **6**. In the case of acetic acid ligands, spectroscopic data and DFT calculations have shown that the acetic acid lies on the metal surface as acetate, together with hydrides.⁴⁹ For the adamantane ligand **2**, DFT calculations have shown that the most stable structure on a Ru_{55} cluster involves the coordination of the two carboxylate moieties on a large facet of the cluster after spontaneous O–H bond activation, with an adsorption energy of –50 and –63 $\text{kcal}\cdot\text{mol}^{-1}$ for the mono- and bi-anchoring coordination mode of the carboxylate group, respectively, see Figure S8 for the latter geometry. However, we assume that a mono-anchoring mode is favored thermodynamically since in that case, more ligands can be adsorbed on the NP surface. For ligands **6**, only the mono-anchoring mode is allowed due to the strong repulsion between surface Ru and the closest hydrogen atoms lying between the two amine groups.

Surface modeling from the analysis of coordination complexes. In order to obtain better insight on the coordination mode of carboxylic acid ligands onto the Ru NP surface we achieved the reaction of $[\text{Ru}(\text{COD})(\text{COT})]$ with **1** and **2**. Reports concerning the reactivity of $[\text{Ru}(\text{COD})(\text{COT})]$ with carboxylic acids have previously shown that reaction with 9-anthracenecarboxylic gives the complex $[\text{Ru}(\eta^9\text{-anthracenecarboxylate})_2(\text{COD})]$,⁵⁸ and with acetic acid gives the Ru complex $[\text{Ru}(\text{CH}_3\text{COO})(\eta^4\text{-1,4-COD})(\eta^5\text{-1,5-COT})]$.⁵⁹ $[\text{Ru}(\text{COD})(\text{COT})]$ reacts smoothly with **1** at room temperature to give $[\text{Ru}(\kappa\text{-AdCOO})(\eta^4\text{-C}_8\text{H}_{12})(\eta^3\text{-C}_8\text{H}_{11})]$ **Ru₁**, isolated as a pale yellow solid in 64% yield and characterized by NMR, IR and X-ray crystallography (see S.1 in the SI).

Ru₁ results from the coordination of the carboxylic acid (see Scheme 3), through oxidative addition of the O–H bond inducing the reduction of cyclooctatriene to form an η^3 -allyl system. Likewise, the coordination of ligand **2** with $[\text{Ru}(\text{COD})(\text{COT})]$ leads to the O–H bond cleavage of the ligand to produce a carboxylate Ru complex. In this case, the presence of two carboxylic acids on the ligand allowed synthesizing a bimetallic complex in which **2** in the carboxylate form acts as a bridge. **Ru₂** was isolated as a yellow powder in 52% yield and characterized by NMR, IR, and elemental analyses (see S.1 in the SI). Similar reactivity, *i.e.* oxidative addition followed by cyclooctatriene reduction, has been reported with Si–H bonds, in which the reduced cyclooctatriene is coordinated to the Ru center through the **Surface coordination chemistry of carboxylic ligands.** In the case of the use of carboxylic stabilizers for NP synthesis, different coordination modes on metallic surface have been reported: i) monodentate; ii) chelating bidentate; and iii) bridging bidentate.⁶⁴ As far as Ru NP stabilized by carboxylate ligands are concerned, Poteau *et al.* reported a bridging bidentate coordination mode ($\Delta\nu = 145 \text{ cm}^{-1}$),⁴⁹ in accordance with data reported for molecular (or polymeric)

three carbons in the allyl form and the two carbons of the double bond.^{60, 61} Upon heating these carboxylate Ru complexes in the presence of ligands, the unsaturated ligands of the Ru center are generally removed. We experimented a similar procedure, *i.e.* heating **Ru₁** at 55 °C in THF in an attempt to reproduce the formation of Ru NP by loss of the unsaturated ligands. A mixture of **1**, **Ru₁**, and other species was obtained. Crystals grown from a saturated solution of the mixture in THF, which correspond to a bimetallic complex **Ru₃**. Single-crystal XRD analysis showed that **Ru₃** contains two ligand **1** coordinated, chelating both metallic centers with a THF molecule attached to one Ru atom (see S.1 in the SI). This finding is in line with the formation of Ru NP by the coordination of ligand **1** to the Ru NP surface. In the two isolated Ru complexes bearing ligands **1** and **2**, the carboxylic acids are easily deprotonated and the carboxylate ligands are chelating bidentate. Complexes **Ru₁** and **Ru₂** show in their IR spectra the typical $\nu_{\text{as}}(\text{COO}^-)$ and $\nu_{\text{s}}(\text{COO}^-)$ bands of the carboxylate ligand at 1497/1443 and 1502/1430 cm^{-1} , respectively. In IR, the difference in $\nu_{\text{as}}(\text{COO}^-)$ and $\nu_{\text{s}}(\text{COO}^-)$ ($\Delta\nu$), is generally used to determine the coordination mode of the carboxylate group. In that case, the $\Delta\nu$ are 54 and 72 cm^{-1} for **Ru₁** and **Ru₂**, respectively, which is in accordance with a chelating bidentate coordination ($\Delta\nu < 110 \text{ cm}^{-1}$).⁶² The ^{13}C NMR spectra of these complexes show singlets at 190.3 and 189.5 ppm for **Ru₁** and **Ru₂**, respectively, attributed to the chelating bidentate carboxylates, which are consistent with chemical shifts reported in the literature for Ru complexes bearing chelating bidentate acetate ligands.⁶³



Scheme 3. Structure of complexes **Ru₁₋₃** isolated from reaction of $[\text{Ru}(\text{COD})(\text{COT})]$ with ligands **1** and **2**.

Ru species bearing such ligands.^{65–68} In Poteau's work, the ^{13}C NMR spectrum of the NP show a singlet at 186 ppm attributed to the acetate. Interestingly, a low intensity band at 1950 cm^{-1} is also observed, attributed to a ν_{CO} band; the CO ligand presumably arising from THF (the reaction solvent) decomposition. XPS, IR, and SS-NMR analyses were performed on the final compound **Ru@2** prepared from ligand **2**. The O1s XPS spectrum of **Ru@2** (Ru/ligand ratio =

10, Figure S6) shows a main peak at 532.2 eV, which can be assigned to deprotonated carboxylic acids.⁶⁹

The IR spectra of **Ru@2** materials prepared at different Ru/L ratio are shown in Figure S9 and compared to the one of the free ligand (Figure 3a shows the spectrum obtained for a Ru/ligand ratio of 10). First, it is clear that like in the coordination complexes, the ligand **2** has been deprotonated since no carboxylic acid (-C=OOH) stretching vibration bands are visible at 1710 cm^{-1} . Whatever the Ru/L ratio, several bands are visible in the $1600\text{-}1300\text{ cm}^{-1}$ region. First, as in the case of Ru NP stabilized by acetate ligands,⁴⁹ we identified bands at $1560/1390\text{ cm}^{-1}$ ($\Delta\nu = 170\text{ cm}^{-1}$), which are consistent with bridging bidentate carboxylate ligands. DFT calculations performed on a $\text{Ru}_{13}\text{H}_{18}@\text{(Ad-COOH-COO}^-)$ model predicted bands at 1473 and 1340 cm^{-1} ($\Delta\nu = 133\text{ cm}^{-1}$). The frequency of the $\nu_{\text{as}}(\text{COO}^-)$ mode is underestimated in our calculation, similarly to reported elsewhere.⁴⁹ Other bands are visible at 1450 , 1361 , 1337 and 1312 cm^{-1} . The band at 1450 cm^{-1} is characteristic of CH_2 scissoring. These bands are not consistent with the presence of monodentate carboxylate species, since monodentate species should give a $\Delta\nu > 200\text{ cm}^{-1}$. DFT calculations performed on a $\text{Ru}_{13}\text{H}_{18}@\text{Ad}(\text{COOH})_2$ model predicted bands at 1590 and 1309 cm^{-1} ($\Delta\nu = 281\text{ cm}^{-1}$). Additionally, monodentate carboxylate Ru complexes give bands for the $\nu_{\text{as}}(\text{COO}^-)$ mode at around 1600 cm^{-1} .⁶⁴ Although it is difficult at that point to safely assign these bands, we can propose the presence of chelate bidentate species. Beside to the bands attributed to carboxylate species, a band at $1940\text{-}1960\text{ cm}^{-1}$ (according to the Ru/ligand ratio) is also observed, as in the work of Poteau *et al.*⁴⁹ In our case, however the intensity of this ν_{CO} band is very high, and depends on the Ru/ligand ratio. At a Ru/ligand ratio of 5, two bands are visible at 2040 and 1942 cm^{-1} ; for a ratio of 10 a single broad band at 1962 cm^{-1} is observed (Figure 3b), and at a ratio of 20 the band at 1957 cm^{-1} is very broad with a shoulder at 1800 cm^{-1} (Figure S9), which could correspond to bridged CO.⁶⁸ The shift of the main band as well as the appearance of new bands could be due to an influence of the CO coverage.⁷⁰⁻⁷³ The origin of CO in the medium will be discussed in the next section. The ^{13}C SS-NMR spectrum of **Ru@2** (Figure 3c) has been recorded on a compound prepared with ^{13}C labeled **2** ($\text{Ad-}^{13}\text{COOH}$) in order to obtain clear signals of the sp^2 carbons of carbonyl groups. Beside the peak at 27.1 ppm corresponding to the sp^3 carbons of the adamantane cage, carbonyl species are detected at 178.3 , 193.6 and 220.1 ppm , which have been attributed to the bridging bidentate carboxylate ligands (186.0 ppm in the work of Poteau *et al.*⁴⁹ and 196.5 ppm in **Ru₃**), whereas the peak at 178.3 ppm could be tentatively attributed to chelate bidentate species (a peak at 185.2 ppm was also observed in the mixture of **Ru₃** synthesis). ^{13}C -NMR studies on Ru complexes bearing chelate bidentate carboxylate ligands have reported We recorded the infrared spectra for which a shift should be observed in the ν_{CO} band if the ^{13}CO comes from the ligand. Figure S11 show the spectra obtained with unlabeled and

chemical shifts ($182\text{-}186\text{ ppm}$), which are consistent with this attribution.⁶⁴

Room temperature carboxylic acid decarbonylation induced by reactive Ru species. The presence of CO ligands on the Ru NP was rather surprising regarding the intensity of the CO band and the origin of their formation. Chaudret *et al.*⁷⁴⁻⁷⁵ and Poteau *et al.*⁴⁹ have also observed the presence of CO ligands on Ru NP that were formed in THF solvent from $[\text{Ru}(\text{COD})(\text{COT})]$. They have attributed this CO formation to the decomposition of THF into propane and CO. Herein, CO could arise either from THF decomposition or from the decarbonylation of **2**. To determine whether the CO arises from ligand **2** or THF, we performed the reaction with labeled **2** using $\text{Ad-}^{13}\text{COOH}$, with a Ru/ligand ratio = 10.

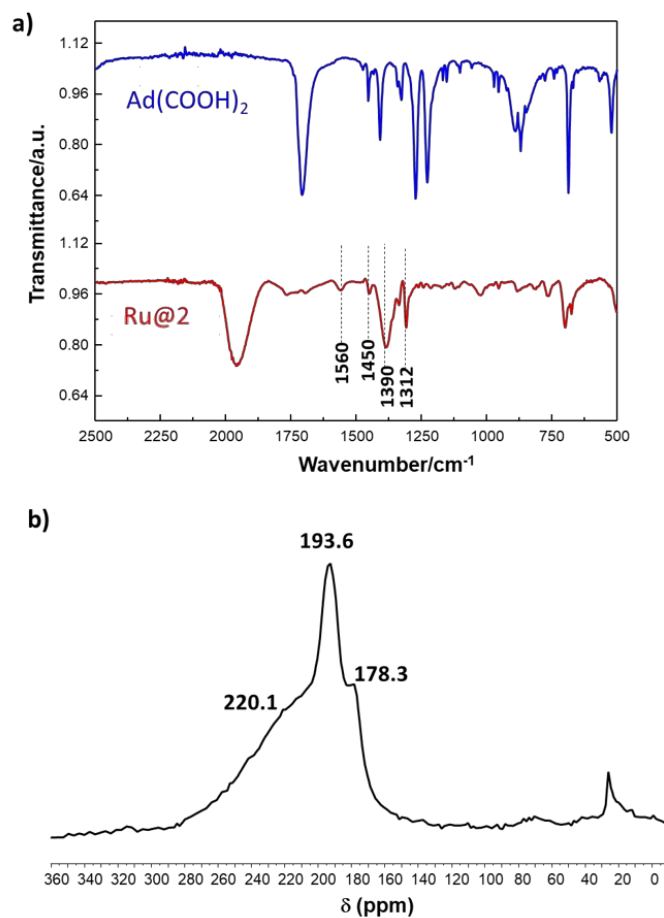


Figure 3. a) IR spectra of **2** and **Ru@2** (Ru/ligand ratio = 10), and b) ^{13}C SS-NMR spectrum of **Ru@2** (Ru/ligand ratio = 10) obtained with a ^{13}C labeled **2** ($\text{Ad-}^{13}\text{COOH}$).

labeled **2**. The CO band for the unlabeled **2** is observed at 1962 cm^{-1} , whereas for the labeled **2** the ν_{CO} band is found at 1934 cm^{-1} . When $^{12}\text{C}^{16}\text{O}$ is replaced by $^{13}\text{C}^{16}\text{O}$ ($R = 0.978$), the

differences between observed and calculated frequencies are generally low. In our case, the calculated frequency should be at 1918 cm^{-1} , so the difference (16 cm^{-1}) is relatively large. This could be because, in addition to ligand **2** decarbonylation, we may also observe some THF decomposition. The large envelopes at 1934 cm^{-1} could encompass two bands ($\text{Ru}^{(13\text{CO})}(^{12}\text{CO})$); the $\text{Ru}^{(13\text{CO})}$ arising from **2** decarbonylation and the $\text{Ru}^{(12\text{CO})}$ from THF decomposition. The fact that THF decomposition also occurs during the reaction of $[\text{Ru}(\text{COD})(\text{COT})]$ with H_2 and polymantane ligands is supported by a ν_{CO} band at $1914\text{--}1923\text{ cm}^{-1}$ that was also observed in the case of the diamine ligands **5**, **6**, **7** and **8** (Figure S12). Decarbonylation of a carboxylic acid at room temperature in the presence of dihydrogen is very surprising since this reaction usually occurs on catalysts at much higher temperature. Accordingly, the decarbonylation of propanoic acid in the presence of H_2 on Ru catalyst has been observed above $180\text{ }^\circ\text{C}$,^{76, 77} in processes rationalized by the energy barrier necessary to pass for C–C bond breaking, as an essential step to produce CO.⁷⁷ This decarbonylation, operated at room temperature, suggests an unanticipated high reactivity of under-coordinated Ru species that are formed during the decomposition of $[\text{Ru}(\text{COD})(\text{COT})]$ in the presence of H_2 and **2**. A DFT study was performed on a Ru_3H_{16} model, as representative species of a small-size reactive intermediate under realistic conditions, where the ligand **2** was replaced by CH_3COOH for simplicity. Several reaction pathways were considered (Figure 4), and the lowest energy routes are discussed below.

The reference initial state is given by those two species infinitely separated. The reaction begins by the thermodynamically favorable coordination of CH_3COOH (-23 kcal.mol^{-1}). We show below that in an energetically favorable process $\text{CO}@_{\text{Ru}_3\text{H}_{16}}$ may form with the assistance of an extra H_2 , and the release of one H_2O and one CH_4 (-46 kcal.mol^{-1}). This pathway is reasonable in terms of kinetics and thermodynamics. In this case, the reaction occurs first through the facile (10 kcal.mol^{-1}) C–OH bond dissociation, leading to the formation of CH_3CO^* and OH^* on the NP. A C–C bond breaking with a lower barrier height (5 kcal.mol^{-1}) follows this step. Yet, this $(\text{CH}_3)^*(\text{CO})^*(\text{OH})^*$ intermediate is slightly less stable than the previous one (-35 vs. -43 kcal.mol^{-1}). Owing to the experimental conditions, under H_2 pressure, one H_2 can easily react on the surface, and act as a thermodynamic driving force leading to the release of CH_4 and H_2O yielding the final adsorbed CO product (-46 kcal.mol^{-1}). Another plausible pathway is a direct C–C dissociation, assuming that mobile surface hydrides allow for the clearance of a facet composed by three Ru atoms. The corresponding energy barrier is 29 kcal.mol^{-1} , when the $(\text{CH}_3)^*(\text{COOH})^*@_{\text{Ru}_3\text{H}_{16}}$ final state remaining high in energy (-1 kcal.mol^{-1}). A second possible pathway is a further dissociation of the carboxylic group (almost barrierless) that yields a very deep well in the potential energy landscape ($(\text{CH}_3\text{COO})^*(\text{H})^*$: -52 kcal.mol^{-1}). This value is slightly lowered compared to the one reported above for **1**@ Ru_3 . This is mainly due to the surface saturation by hydrides. This

intermediate corresponds to a thermodynamic trap since neither a further C–C nor C–O dissociation could provide a more stable state. The question thus arising is which principle reaction favor the CO formation herein. Some reported semi-quantitative clues based on previous phase diagrams calculations are to be considered.^{49, 78} These diagrams show that under realistic conditions close to the ones we used, a Ru_{55} NP in the presence of acetic acid and CO pressure can respectively accommodate 16 $(\text{CH}_3\text{COO})^*(\text{H})^*$ and up to 63 $(\text{CO})^*$. Owing to the average adsorption energy per ligand (-35 kcal.mol^{-1} per $(\text{CH}_3\text{COO})^*(\text{H})^*$ and -40 kcal.mol^{-1} per $(\text{CO})^*$), the final decomposition of a large amount of acids into CO can be considered as the strongest driving force. It is however worth noting that to turn this unexpected reactivity into a catalytic reaction at low temperature, the system has to face the very strong CO adsorption at the Ru NP surface, which may block the catalytic activity of the Ru centers.

Overall, the results from structural characterization and surface coordination chemistry studies demonstrate, for the first time, that bifunctional rigid polymantane ligands with well-defined functionalization (functions and their position) promote the synthesis of unprecedented Ru NP networks in which are well controlled both Ru NP size uniformity and interparticle distances. Because of the relatively low cost and good availability of Ru among precious metals, we investigated the Ru NP network catalytic performances for an atom-economic hydrogenation reaction, with the additional aims of providing high catalytic selectivity and evidencing structure/performance relationship.

Ru NP network activity in catalytic hydrogenation of phenylacetylene. The selective hydrogenation of alkynes to alkenes is a particularly valuable reaction in synthetic organic chemistry. The hydrogenation of phenylacetylene in liquid phase is a benchmark method for assessing catalytic activity and selectivity of Pd NP.⁷⁹ Although there is a need for selective hydrogenation catalysts that are less expensive than conventional Pd-based catalysts, Ru NP have been little studied.^{80–87} For this reaction, the catalytic properties of the transition metal strongly depend on its electronic structure. The catalytic behavior of Ru NP prepared with the different polymantane ligands was studied in the hydrogenation of phenylacetylene into styrene at room temperature and a constant H_2 pressure of 5 bar (Table 2, entries 1–11). The evolution of activity and selectivity over time (Figure S13) shows that for most of the catalysts, at the exception of the less active **Ru@4**, the styrene selectivity decreases abruptly at high conversions due to the formation of ethylbenzene and ethyl cyclohexane, resulting from the complete hydrogenation of the phenyl ring. Product distribution over time is shown on Figure S14 for **Ru@1**, **Ru@2**, **Ru@5** and **Ru@6** (Ru/ligand = 10). The hydrogenation of arenes under mild reaction conditions using (supported or colloidal) Ru NP as catalysts has already been reported,^{88–91} and is not surprising, even at room temperature.

1
2
3
4
5
6
7
8
9
10
11
12
13
14
15
16
17
18
19
20
21
22
23
24
25
26
27
28
29
30
31
32
33
34
35
36
37
38
39
40
41
42
43
44
45
46
47
48
49
50
51
52
53
54
55
56
57
58
59
60

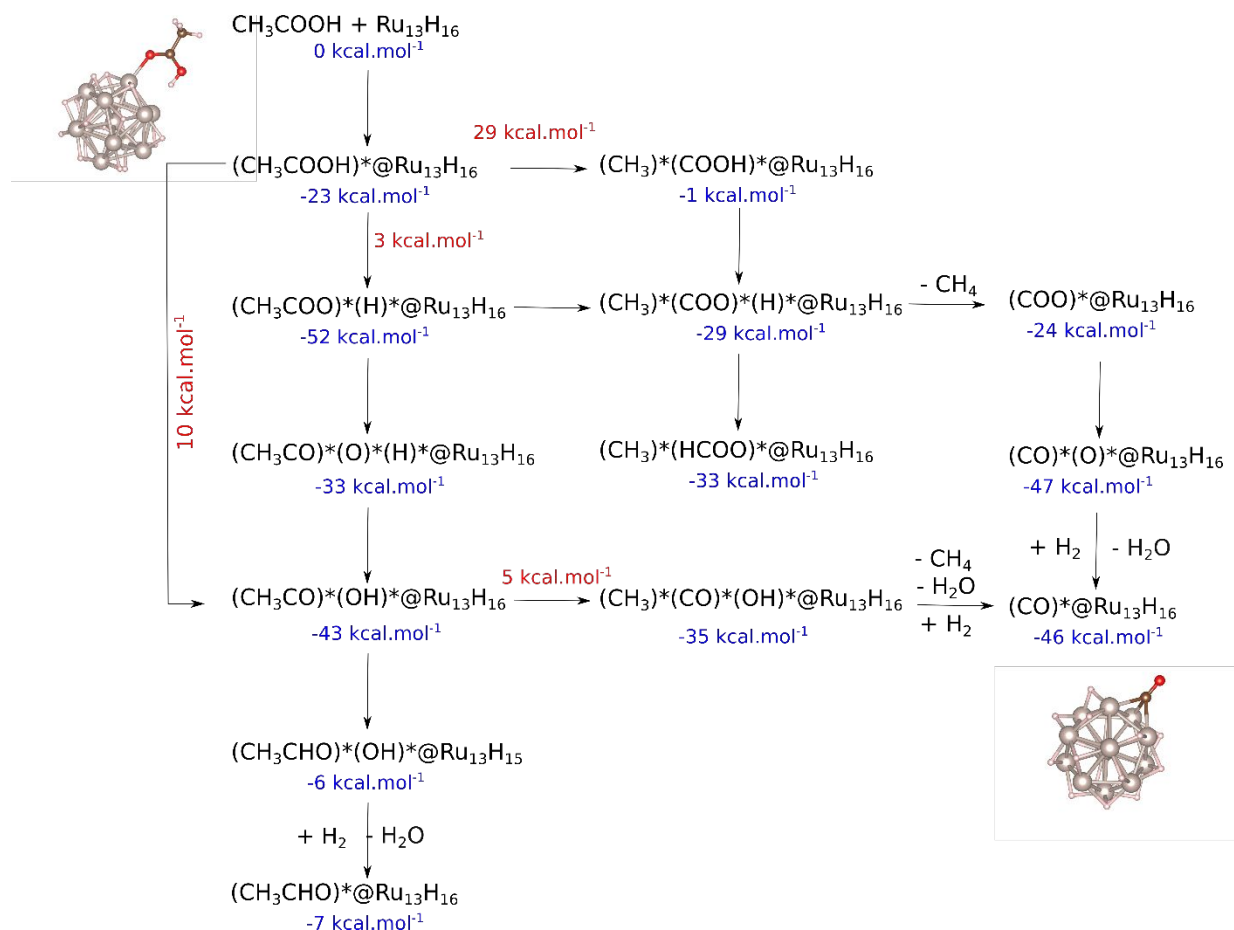


Figure 4. DFT investigation of decarbonylation's reaction mechanism. Blue values correspond to total energy differences with respect to the initial state, when red ones give energy barrier height.

Figure 5a shows the calculated TOF according to the nature of the ligand. For each series of ligands (acids and amines), the use of discrete Ru NP (from **1** and **5**, adamantane monoacid and monoamine, respectively) provides higher TOF than the use of Ru NP networks (from **2** and **6**, adamantanes, and **4** and **8**, diamantanes, diacids and diamines, respectively). We independently checked that this result cannot be rationalized by the amount of adsorbed polymantane ligands (Table S1) on the NP surface. Considering that diffusion limitations should not be limiting in our case since catalytic activity is low (in the h^{-1} range) and the catalytic particles are small (in the sub-micrometric range), this result can rely on an important difference between these materials, which is the presence of significant amount of adsorbed CO on the Ru NP networks. This adsorbed CO poisons the Ru NP in the network, which are finally less active than the discrete NP. Additional experiments were performed to validate this hypothesis. We tested as catalyst a Ru NP network ($\text{Ru}^*\text{@2} - 10/1$) that have been vacuum treated to remove the adsorbed CO, and compared the TOF at 100% conversion of $\text{Ru}@1 - 10/1$, $\text{Ru}@2 - 10/1$ and $\text{Ru}^*\text{@2} - 10/1$. The TOF obtained were respectively 113.8, 101.9, and 117.4 h^{-1} . From Figure 5a, it is discernible that

the use of donating amino ligands (**5-8**) allows reaching higher TOF than with the carboxylic ligands. The fact that amine ligands, which insure a higher electronic density on Ru, allow reaching higher TOF for phenylacetylene hydrogenation is in accordance with results reported in the literature. Thus, it was reported that for the hydrogenation of various unsaturated compounds on stabilized Ru NPs, the use of σ -donor ligands increases the activity of the Ru NP.⁹²⁻⁹³ Similarly, Ru/N-doped carbon catalysts were reported to be very efficient catalysts for arene hydrogenation.⁹⁴

We assume that the amine as σ -donor ligand increases the electron density at the NP surface, favoring thus the π -back donation from the d Ru orbitals to the antibonding π^* orbital of the alkyne/alkene, which facilitates rapid hydrogenation. Accordingly, a slightly higher selectivity towards styrene was observed when using carboxylic acid ligands (Figure 5b). Indeed, in that case, the charge transfer from the metal to the ligand results in electro-deficient Ru NP that provide less π -back donation to the alkene, which weakens Ru-alkene bonding and favors its quick desorption, thus avoiding overhydrogenation to produce ethylbenzene.

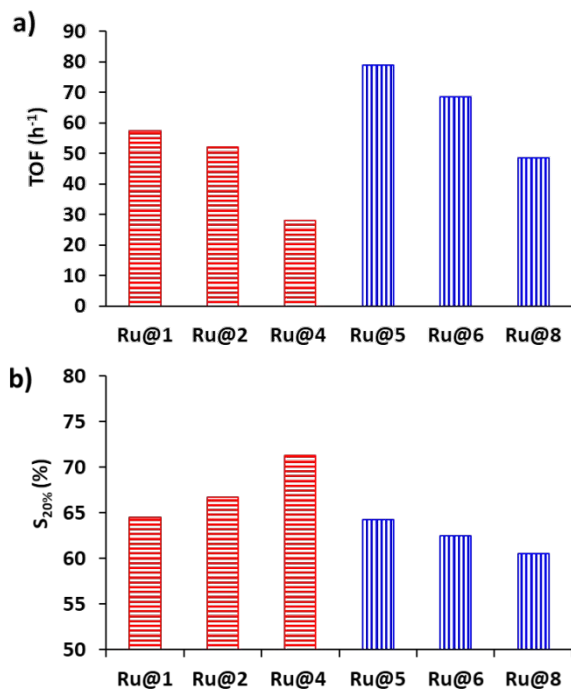


Figure 5. a) Activity, and b) styrene selectivity at 20% conversion for catalysts **Ru@1**, **Ru@2**, **Ru@4**, **Ru@5**, **Ru@6** and **Ru@8** (Ru/ligand = 10/1). Red horizontal lines = carboxylic ligands; and blue vertical lines = amine ligands.

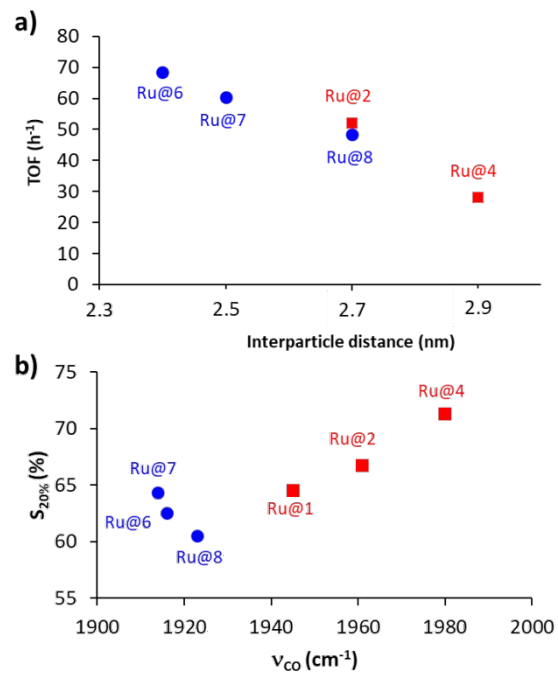
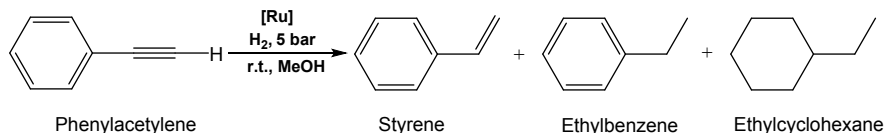


Figure 6. a) Activity (TOF calculated according to surface Ru content) as a function of the interparticle distance, and b) styrene selectivity at 20% conversion as a function of the ν_{CO} frequency of CO adsorbed on the catalysts (blue spheres amine ligands, and red squares acid ligands). The Ru/ligand ratio in these catalysts is 10/1.

Table 2. Hydrogenation of phenylacetylene catalyzed by Ru catalysts.^{a)}



Entry	Catalysts	Time (h)	Conv. (%)	S _{20%} (%)	S _{60%} (%)	TOF (h ⁻¹) ^a
1	Ru@1 - 5/1	2	84.4	62.3	58.3	61.6
2	Ru@1 - 10/1	3	73.1	64.5	61.5	112.9
3	Ru@1 - 20/1	4	73.2	63.5	61.7	45.6
4	Ru@2 - 5/1	4	66.7	68.9	66.7	30.3
5	Ru@2 - 10/1	3	71.6	66.7	63.6	64.9
6	Ru@2 - 20/1	3	79.1	66.7	63.6	74.2
7	Ru@4 - 10/1	5	62.1	71.3	65.4	18.9
8	Ru@5 - 10/1	2	72.7	64.3	59.6	98.7
9	Ru@6 - 10/1	2	65.9	62.5	58.9	101.4
10	Ru@7 - 10/1	3	72.6	65.2	64.9	66.6
11	Ru@8 - 10/1	3	66.8	60.5	56.3	74.9
12	1.6%Ru/O-CNT	8	10.6	67.8 ^b	-	-
13	0.8%Ru/N-CNT	4	9.0	67.4 ^b	-	-

Reaction conditions: 0.02 mmol Ru, 412 mg (4.00 mmol) phenylacetylene, 71 mg (0.50 mmol) decane (internal standard), room temperature, 5 bar H₂, 25 mL MeOH. a TOF calculated according to surface Ru content at 1 h reaction. b Selectivity given at 10% of conversion.

In a series of ligand (acid or amines) providing Ru NP network, some differences can also be noted. The use of bulkier ligands such as BAd and DAd is detrimental to the activity. We also observed a positive confinement effect in relation with shorter interparticle distances. Notably, the interparticle distance is not affected by changes in Ru NP size since all the catalysts present very similar size (1.7-1.9 nm). Whatever the type of ligand a correlation between the interparticle distance and the catalyst activity is indicated by the analysis of Figure 6a: the closer the particles the higher the activity. The effects of confinement in carbon materials have been identified as possible levers to modify catalytic performances.⁹⁵ It has been shown that soft confinement effects, such as reactant enrichment or rapid diffusion, will directly affect the kinetics of the reaction. Hard effects, like the charge transfer between the metal and the support, will also affect activity/selectivity and stability. In our case, the lower is the interparticle distance, thus giving more confined Ru NP, higher is the activity. A correlation can also be drawn between the interparticle distance and selectivity (Figure 6b) considering both amine and acid as ligands, which is reverse to the correlation observed between interparticle distance and activity. Larger distance induces a decrease of the activity; in that case styrene could be desorbed before further hydrogenation, leading to higher selectivity. Considering that reactant concentration enrichment (as well as high diffusion rates) have been regularly reported as explanation of "soft" confinement effects, we preferred to rely on this explanation. It should nevertheless be noted that the search for a detailed explanation of the observed confinement effects would require a study in itself, which falls outside the scope of our study. Additionally, in acid or amines series no evident correlation was found between the NP size and their activity. Considering the surface electronic density, which was probed via the ν_{CO} frequency of CO adsorbed on the catalysts after their synthesis and theoretically, we find a correlation for the acid series as far as activity and selectivity a concerned (Figure S15). As expected, we can notice an increase of the selectivity and a decrease of the activity when the electronic density on the Ru NP is decreased (higher ν_{CO} frequency). For the σ -donor amine ligands, which provide a higher electronic density on the Ru NP, the selectivity is lower. However, differences of ν_{CO} shifts between the amine ligands are too close to allow drawing any general correlation (Figure S15). It is nevertheless important to note that in this series appears the ligand **7**, which presents a more flexible backbone than the other ligands, which could also explain this lack of correlation. Indeed, if this ligand is disregarded, the same type of tendency as for the ligands of the acid series is observed.

We also compared the stability of catalysts prepared from amine and carboxylic ligands. The Figure S16 shows TEM micrographs of the fresh and spent catalysts. It is clear from this figure that the networks prepared from acid ligands

provide more robust catalysts, as expected from the DFT calculations (Figure S2). While an influence of the solvent for adsorption (and ligand displacement) or swelling of the networks in the course of catalytic reactions could not be completely ruled out, Ru NP networks were not found to be significantly modified after catalysis suggesting a rather robust/rigid framework.

Finally, to better delineate the performances of the Ru NP and NP networks prepared from the functionalized polymantane ligands we compared their reactivity with the ones of individual unprotected Ru NP deposited on functionalized carbon nanotubes (CNT). Two types of CNT were used, CNT functionalized with nitric acid (O-CNT) that contains significant amounts of carboxylic groups to stabilize Ru NP,⁴⁷ and CNT prepared from acetonitrile, which contains different types of nitrogen groups (N-CNT), such as pyridinic or amines.⁹⁶ Both catalysts present similar Ru NP size (1-2 nm) and show much lower conversions (Table 2, entries 12 and 13) than the NP networks. However, the same tendency as the one observed for the Ru NP networks was observed, *i.e.* a higher activity is obtained with the catalyst containing nitrogen functionalities. As for the Ru NP networks at low conversion (Figure S14), these two Ru/CNT catalysts show similar selectivity. The higher activity obtained with Ru NP networks nicely illustrate the interest provided from rigid polymantane ligands in Ru-catalyzed hydrogenation. These also hold promises concerning the use of NP networks in relation with inedited confinement effects in which short-range interactions between NP may greatly improve their catalytic activity.

CONCLUSIONS

We have successfully prepared catalytic materials based on well-defined small nanometric-sized Ru NP (< 2 nm) stabilized by mono or difunctionalized adamantanes, bis-adamantanes and diamantanes, bearing either carboxylic acid or amine functional groups. Unprecedented assembling of networks based on polymantanes are described. We have shown that the interparticle distances can be tuned by a proper choice of the ligand and the Ru/ligand ratio. We have also shown that the choice of the ligand is crucial to tune the electronic properties of the metal. In a systematic approach from molecular regime to NP and networks, the coordination chemistry of these species has been investigated, and it was shown that highly reactive Ru clusters or colloidal species are formed during NP network synthesis, which were experimentally shown to be able to decarbonylate carboxylic acids at room temperature in the presence of 3 bar of H₂. DFT theoretical investigation, which supported this high reactivity with small clusters, also allowed proposing a preferential low energy pathway for this innovative decarbonylation reaction.

These new nanoparticle networks constitute a unique set to investigate structural and electronic effects in

heterogeneous catalysis with flexible assembly of nano-objects, especially confinement effects were revealed that exalt catalytic activity. In the hydrogenation of phenyl acetylene we evidenced that Ru NP interparticle distance and electronic effects control the catalyst activity; whereas electronic effects mainly govern the catalyst selectivity.

ASSOCIATED CONTENT

Supporting Information. This material is available free of charge via the internet at <http://pubs.acs.org>.

It contains, materials synthesis and characterization by ICP, XPS, IR, SAXS, WAXS, optimized geometry from DFT, and data related to phenyl acetylene hydrogenation.

AUTHOR INFORMATION

Corresponding Author

*E-mail: Philippe.serp@lcc-toulouse.fr.

Author Contributions

Y. M. synthesized and participated to the characterization of the 3D ruthenium nanoparticle covalent assemblies and performed the catalytic studies. H.N. designed the global synthetic pathways of polymantane ligands and achieved most of the late-stage functionalization for polymantane ligands. D.P. synthesized and characterized the precursors for functionalized polymantane ligands. P.L. performed the WAXS analyses and interpreted the results. Y. T. and H. M. performed the XPS analyses and interpreted the results. P. R. performed the SAXS analyses and interpreted the results. A.F. performed the electron tomography characterization. R. P., I. del R. and I. Gerber performed the DFT calculations. J.C. H. supervised the work on polymantane ligands synthesis and contributed to catalysis discussion. M. R. A. participated to the supervision of the work on 3D ruthenium nanoparticle covalent assemblies and catalytic studies. P. S. conceived the idea of 3D ruthenium nanoparticle covalent assembly synthesis for catalytic applications and coordinated the entire work.

All authors have given approval to the final version of the manuscript.

Funding Sources

This work was supported by the Agence Nationale de la Recherche (ANR project ANR-16-CE07-0007-01, Icare-1), which is gratefully acknowledged. I.C.G. acknowledges the *Calcul en Midi-Pyrénées* initiative, CALMIP (Project p0812), for computer time allocation. This work was also granted access to the HPC resources of CINES and IDRIS under the allocation 2019-A0060906649 made by GENCI. In Dijon, the work was supported by the CNRS, Université de Bourgogne, Conseil Régional de Bourgogne through the plan d'actions régional pour l'innovation (PARI) and the fonds européen de développement regional (FEDER) programs.

Notes

The authors declare no competing financial interest.

ACKNOWLEDGMENT

This research used resources of the Core Labs of KAUST, and Dr. Thomas Theussl, scientist at KAUST Visualization Core Lab, is gratefully acknowledged for developing the codes that allowed the ET data analysis.

ABBREVIATIONS

CCR2, CC chemokine receptor 2; CCL2, CC chemokine ligand 2; CCR5, CC chemokine receptor 5; TLC, thin layer chromatography.

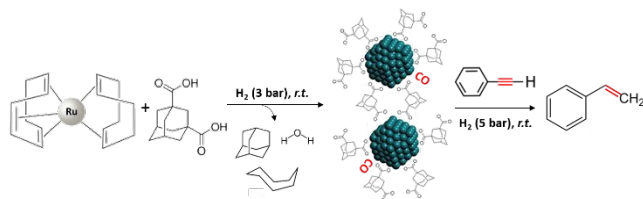
REFERENCES

- (1) Fendler, J. H. Self-Assembled Nanostructured Materials. *Chem. Mater.* **1996**, *8*, 1616-1624.
- (2) Fendler, J. H. Chemical Self-Assembly for Electronic Applications. *Chem. Mater.* **2001**, *13*, 3196-3210.
- (3) Vriezema, D. M.; Comellas Aragonès, M.; Elemans, J. A. A. W.; Cornelissen, J. J. L. M.; Rowan, A. E.; Nolte, R. J. M. Self-Assembled Nanoreactors. *Chem. Rev.* **2005**, *105*, 1445-1490.
- (4) Boles, M. A.; Engel, M.; Talapin, D. V. Self-Assembly of Colloidal Nanocrystals: From Intricate Structures to Functional Materials. *Chem. Rev.* **2016**, *116*, 11220-11289.
- (5) Lu, C.; Tang, Z. Advanced Inorganic Nanoarchitectures from Oriented Self-Assembly. *Adv. Mater.* **2016**, *28*, 1096-1108.
- (6) Wang, L.; Xu, L.; Kuang, H.; Xu, C.; Kotov, N. A. Dynamic Nanoparticle Assemblies. *Acc. Chem. Res.* **2012**, *45*, 1916-1926.
- (7) B Sohn, B.-H.; Choi, J.-M.; Yoo, S. I.; Yun, S.-H.; Zin, W.-C.; Jung, J. C.; Kanehara, M.; Hirata, T.; Teranishi, T. Directed Self-Assembly of Two Kinds of Nanoparticles Utilizing Monolayer Films of Diblock Copolymer Micelles. *J. Am. Chem. Soc.* **2003**, *125*, 6368-6369.
- (8) Shen, Z.; Yamada, M.; Miyake, M. Control of Stripelike and Hexagonal Self-Assembly of Gold Nanoparticles by the Tuning of Interactions between Triphenylene Ligands. *J. Am. Chem. Soc.* **2007**, *129*, 14271-14280.
- (9) Kanehara, M.; Kodzuka, E.; Teranishi, T. Self-Assembly of Small Gold Nanoparticles through Interligand Interaction. *J. Am. Chem. Soc.* **2006**, *128*, 13084-13094.
- (10) Rousseau, G.; Lavenn, C.; Cardenas, L.; Lorient, S.; Wang, Y.; Hahn, U.; Nierengarten, J.-F.; Demessence, A. One-Pot Synthesis of Sub-3 Nm Gold Nanoparticle Networks Connected by Thio-Based Multidentate Fullerene Adducts. *Chem. Commun.* **2015**, *51*, 6730-6733.
- (11) Leng, F.; Gerber, I. C.; Lecante, P.; Bentaleb, A.; Muñoz, A.; Illescas, B. M.; Martín, N.; Melinte, G.; Ersen, O.; Martinez, H. *et al.* Hexakis [60]Fullerene Adduct-Mediated Covalent Assembly of Ruthenium Nanoparticles and Their Catalytic Properties. *Chem. Eur. J.* **2017**, *23*, 13379-13386.
- (12) Abbas, A.; Kattumenu, R.; Tian, L.; Singamaneni, S. Molecular Linker-Mediated Self-Assembly of Gold Nanoparticles: Understanding and Controlling the Dynamics. *Langmuir* **2013**, *29*, 56-64.
- (13) Meyer, R. J.; Zhang, Q.; Kryczka, A.; Gomez, C.; Todorovic, R. Perturbation of Reactivity with Geometry: How Far Can We Go? *ACS Catal.* **2018**, *8*, 566-570.
- (14) Axet, M. R.; Dechy-Cabaret, O.; Durand, J.; Gouygou, M.; Serp, P. Coordination Chemistry on Carbon Surfaces. *Coord. Chem. Rev.* **2016**, *308*, 236-345.
- (15) Axet, M. R.; Durand, J.; Gouygou, M.; Serp, P. In *Advances in Organometallic Chemistry*; Pérez, P. J., Ed.; Elsevier Academic Press: Cambridge, MA, USA, **2019**; Vol. 71, pp. 53-174.
- (16) Serp, P. In *Comprehensive Inorganic Chemistry II (Second*

- Edition); Reedijk, J.; Poepelmeier, K., Eds.; Elsevier: Amsterdam, **2013**, Vol. 7, pp 323-369.
- (17) Campisi, S.; Chan-Thaw, C. E.; Villa, A. Understanding Heteroatom-Mediated Metal-Support Interactions in Functionalized Carbons: A Perspective Review. *Appl. Sci.* **2018**, *8*, 1159.
- (18) Chen, P.; Chew, L. M.; Kostka, A.; Muhler, M.; Xia, W. The Structural and Electronic Promoting Effect of Nitrogen-Doped Carbon Nanotubes on Supported Pd Nanoparticles for Selective Olefin Hydrogenation. *Catal. Sci. Technol.* **2013**, *3*, 1964-1971.
- (19) Schwertfeger, H.; Fokin, A. A.; Schreiner, P. R. Diamonds Are a Chemist's Best Friend: Diamondoid Chemistry Beyond Adamantane. *Angew. Chem. Int. Ed.* **2008**, *47*, 1022-1036.
- (20) Gunawan, M. A.; Hierso, J.-C.; Poinso, D.; Fokin, A. A.; Fokina, N. A.; Tkachenko, B. A.; Schreiner, P. R. Diamondoids: Functionalization and Subsequent Applications of Perfectly Defined Molecular Cage Hydrocarbons. *New J. Chem.* **2014**, *38*, 28-41.
- (21) Nasrallah, H.; Hierso, J.-C. Porous Materials Based on 3-Dimensional Td-Directing Functionalized Adamantane Scaffolds and Applied as Recyclable Catalysts. *Chem. Mater.* **2019**, *31*, 619-642.
- (22) Olah, G. A.; Ramaiah, P.; Rao, C. B.; Sandford, G.; Golam, R.; Trivedi, N. J.; Olah, J. A. Electrophilic Reactions at Single Bonds. 25. Nitration of Adamantane and Diamantane with Nitronium Tetrafluoroborate. *J. Am. Chem. Soc.* **1993**, *115*, 7246-7249.
- (23) Moncea, O.; Gunawan, M. A.; Poinso, D.; Cattey, H.; Becker, J.; Yurchenko, R. I.; Butova, E. D.; Hausmann, H.; Šekutor, M.; Fokin, A. A. et al. Defying Stereotypes with Nanodiamonds: Stable Primary Diamondoid Phosphines. *J. Org. Chem.* **2016**, *81*, 8759-8769.
- (24) Yang, W. L.; Fabbri, J. D.; Willey, T. M.; Lee, J. R. I.; Dahl, J. E.; Carlson, R. M. K.; Schreiner, P. R.; Fokin, A. A.; Tkachenko, B. A.; Fokina, N. A. et al. Monochromatic Electron Photoemission from Diamondoid Monolayers. *Science* **2007**, *316*, 1460-1462.
- (25) Gunawan, M. A.; Moncea, O.; Poinso, D.; Keskes, M.; Domenichini, B.; Heintz, O.; Chassagnon, R.; Herbst, F.; Carlson, R. M. K.; Dahl, J. E. P. et al. Nanodiamond-Palladium Core-Shell Organohybrid Synthesis: A Mild Vapor-Phase Procedure Enabling Nanolayering Metal onto Functionalized Sp³-Carbon. *Adv. Funct. Mater.* **2018**, *28*, 1705786.
- (26) Moncea, O.; Casanova-Chafer, J.; Poinso, D.; Ochmann, L.; Mboyi, C. D.; Nasrallah, H. O.; Llobet, E.; Makni, I.; El Atrous, M.; Brandès, S. et al. Diamondoid Nanostructures as Sp³-Carbon-Based Gas Sensors. *Angew. Chem. Int. Ed.* **2019**, *58*, 9933-9938.
- (27) Kresse, G.; Furthmüller, J. Efficiency of Ab-Initio Total Energy Calculations for Metals and Semiconductors using a Plane-Wave Basis Set. *Comput. Mater. Sci.* **1996**, *6*, 15-50.
- (28) Kresse, G.; Hafner, J. Ab Initio Molecular Dynamics for Liquid Metals. *Phys. Rev. B* **1993**, *47*, 558-561.
- (29) Kresse, G.; Furthmüller, J. Efficient Iterative Schemes for Ab Initio Total-Energy Calculations using a Plane-Wave Basis Set. *Phys. Rev. B* **1996**, *54*, 11169-11186.
- (30) Kresse, G.; Hafner, J. Ab Initio Molecular-Dynamics Simulation of the Liquid-Metal-Amorphous-Semiconductor Transition in Germanium. *Phys. Rev. B* **1994**, *49*, 14251-14269.
- (31) Blöchl, P. E. Projector Augmented-Wave Method. *Phys. Rev. B* **1994**, *50*, 17953-17979.
- (32) Kresse, G.; Joubert, D. From Ultrasoft Pseudopotentials to the Projector Augmented-Wave Method. *Phys. Rev. B* **1999**, *59*, 1758-1775.
- (33) Perdew, J. P.; Burke, K.; Ernzerhof, M. Generalized Gradient Approximation Made Simple. *Phys. Rev. Lett.* **1996**, *77*, 3865-3868.
- (34) Momma, K.; Izumi, F.: VESTA 3 for Three-Dimensional Visualization of Crystal, Volumetric and Morphology Data. *J. Appl. Crystallogr.* **2011**, *44*, 1272-1276.
- (35) Tang, W.; Sanville, E.; Henkelman, G.: A Grid-Based Bader Analysis Algorithm without Lattice Bias. *J. Phys.: Condens. Matter* **2009**, *21*, 084204/1-084204/7.
- (36) del Rosal, I.; Truflandier, L.; Poteau, R.; Gerber, I. C.: A Density Functional Theory Study of Spectroscopic and Thermodynamic Properties of Surficial Hydrides on Ru (0001) Model Surface: The Influence of the Coordination Modes and the Coverage. *J. Phys. Chem. C* **2011**, *115*, 2169-2178.
- (37) Henkelman, G.; Uberuaga, B. P.; Jonsson, H. A Climbing Image Nudged Elastic Band Method for Finding Saddle Points and Minimum Energy Paths. *J. Chem. Phys.* **2000**, *113*, 9901-9904.
- (38) Henkelman, G.; Jonsson, H. Improved Tangent Estimate in the Nudged Elastic Band Method for Finding Minimum Energy Paths and Saddle Points. *J. Chem. Phys.* **2000**, *113*, 9978-9985.
- (39) Sheppard, D.; Terrell, R.; Henkelman, G. Optimization Methods for Finding Minimum Energy Paths. *J. Chem. Phys.* **2008**, *128*, 134106-1-10.
- (40) Davis, M. C.; Nissan, D. A. Preparation of Diamines of Adamantane and Diamantane from the Diazides. *Synth. Commun.* **2006**, *36*, 2113-2119.
- (41) Senchyk, G. A.; Lysenko, A. B.; Krautscheid, H.; Domasevitch, K. V. "Fluoride Molecular Scissors": A Rational Construction of New Mo(VI) Oxofluorido/1,2,4-Triazole Mofs. *Inorg. Chem. Commun.* **2011**, *14*, 1365-1368.
- (42) Reinhardt, H. F. Biadamantane and Some of Its Derivatives. *J. Org. Chem.* **1962**, *27*, 3258-3261.
- (43) Zhu, X.; Shao, B.; Vanden Bout, D. A.; Plunkett, K. N. Directing the Conformation of Oligo(Phenylenevinylene) Polychromophores with Rigid, Nonconjugatable Morphons. *Macromolecules* **2016**, *49*, 3838-3844.
- (44) Fokina, N. A.; Tkachenko, B. A.; Merz, A.; Serafin, M.; Dahl, J. E. P.; Carlson, R. M. K.; Fokin, A. A.; Schreiner, P. R. Hydroxy Derivatives of Diamantane, Triamantane, and [121]Tetramantane: Selective Preparation of Bis-Apical Derivatives. *Eur. J. Org. Chem.* **2007**, *2007*, 4738-4745.
- (45) Vodička, L.; Janků, J.; Burkhard, J. Synthesis of Diamantanedicarboxylic Acids with the Carboxy Groups Bonded at Tertiary Carbon Atoms. *Collect. Czech. Chem. Commun.* **1983**, *48*, 1162-1172.
- (46) Robinson, I.; Zacchini, S.; Tung, L. D.; Maenosono, S.; Thanh, N. T. K. Synthesis and Characterization of Magnetic Nanoalloys from Bimetallic Carbonyl Clusters. *Chem. Mater.* **2009**, *21*, 3021-3026.
- (47) T Morris, T.; Zubkov, T. Steric Effects of Carboxylic Capping Ligands on the Growth of the Cdse Quantum Dots. *Colloid Surf. A* **2014**, *443*, 439-449.
- (48) Pan, C.; Pelzer, K.; Philippot, K.; Chaudret, B.; Dassenoy, F.; Lecante, P.; Casanove, M.-J. Ligand-Stabilized Ruthenium Nanoparticles: Synthesis, Organization, and Dynamics. *J. Am. Chem. Soc.* **2001**, *123*, 7584-7593.
- (49) Gonzalez-Gomez, R.; Cusinato, L.; Bijani, C.; Coppel, Y.; Lecante, P.; Amiens, C.; del Rosal, I.; Philippot, K.; Poteau, R. Carboxylic Acid-Capped Ruthenium Nanoparticles: Experimental and Theoretical Case Study with Ethanoic Acid. *Nanoscale* **2019**, *11*, 9392-9409.
- (50) L. M. Martínez-Prieto, I. Cano, A. Márquez, E. A. Baquero, S. Tricard, L. Cusinato, I. del Rosal, R. Poteau, Y. Coppel, K. Philippot, B. Chaudret, J. Cámpora, P. W. N. M. van Leeuwen. Zwitterionic Amidates as Effective Ligands for Platinum Nanoparticle Hydrogenation Catalysts. *Chem. Sci.* **2017**, *8*, 2931-2941.

- (51) Martínez-Prieto, L. M.; Chaudret, B. Organometallic Ruthenium Nanoparticles: Synthesis, Surface Chemistry, and Insights into Ligand Coordination. *Acc. Chem. Res.* **2018**, *51*, 376-384.
- (52) Taglang, C.; Martínez-Prieto, L. M.; del Rosal, I.; Maron, L.; Poteau, R.; Philippot, K.; Chaudret, B.; Perato, S.; Sam Lone, A.; Puente, C. et al. Enantiospecific C-H Activation Using Ruthenium Nanocatalysts. *Angew. Chem. Int. Ed.* **2015**, *54*, 10474-10477.
- (53) Tristany, M.; Chaudret, B.; Dieudonné, P.; Guari, Y.; Lecante, P.; Matsura, V.; Moreno-Mañas, M.; Philippot, K.; Pleixats, R. Synthesis of Ruthenium Nanoparticles Stabilized by Heavily Fluorinated Compounds. *Adv. Funct. Mater.* **2006**, *16*, 2008-2015.
- (54) Tricard, S.; Said-Aizpuru, O.; Bouzouita, D.; Usmani, S.; Gillet, A.; Tassé, M.; Poteau, R.; Viau, G.; Demont, P.; Carrey, J. et al. Chemical Tuning of Coulomb Blockade at Room-Temperature in Ultra-Small Platinum Nanoparticle Self-Assemblies. *Mater. Horiz.* **2017**, *4*, 487-492.
- (55) Morgan, D. J. Resolving Ruthenium: XPS Studies of Common Ruthenium Materials. **2015**, *47*, 1072-1079.
- (56) Salas, G.; Santini, C. C.; Philippot, K.; Collière, V.; Chaudret, B.; Fenet, B.; Fazzini, P. F. Influence of Amines on the Size Control of in Situ Synthesized Ruthenium Nanoparticles in Imidazolium Ionic Liquids. *Dalton Trans.* **2011**, *40*, 4660-4668.
- (57) Wood, M. H.; Welbourn, R. J. L.; Charlton, T.; Zorbakhsh, A.; Casford, M. T.; Clarke, S. M. Hexadecylamine Adsorption at the Iron Oxide-Oil Interface. *Langmuir* **2013**, *29*, 13735-13742.
- (58) Machado, B. F.; Oubenali, M.; Rosa Axet, M.; Trang Nguyen, T.; Tunckol, M.; Girleanu, M.; Ersen, O.; Gerber, I. C.; Serp, P. Understanding the Surface Chemistry of Carbon Nanotubes: Toward a Rational Design of Ru Nanocatalysts. *J. Catal.* **2014**, *309*, 185-198.
- (59) Osakada, K.; Grohmann, A.; Yamamoto, A. New Ruthenium Carboxylate Complexes Having a 1-5-Eta.5-Cyclooctadienyl Ligand. *Organometallics* **1990**, *9*, 2092-2096.
- (60) Smart, K. A.; Grellier, M.; Coppel, Y.; Vendier, L.; Mason, S. A.; Capelli, S. C.; Albinati, A.; Montiel-Palma, V.; Muñoz-Hernández, M. A.; Sabo-Etienne, S. Nature of Si-H Interactions in a Series of Ruthenium Silazane Complexes Using Multinuclear Solid-State Nmr and Neutron Diffraction. *Inorg. Chem.* **2014**, *53*, 1156-1165.
- (61) Smart, K. A.; Grellier, M.; Vendier, L.; Mason, S. A.; Capelli, S. C.; Albinati, A.; Sabo-Etienne, S. Step-by-Step Introduction of Silazane Moieties at Ruthenium: Different Extents of Ru-H-Si Bond Activation. *Inorg. Chem.* **2013**, *52*, 2654-2661.
- (62) Jopes, J. C. S.; Damasceno, J. L.; Oliveira, P. F.; Guedes, A. P. M.; Tavares, D. C.; Deflon, V. M.; Lopes, N. P.; Pivatto, M.; Batista, A. A.; Maia, P. I. S. et al. Ruthenium(II) Complexes Containing Anti-Inflammatory Drugs as Ligands: Synthesis, Characterization and in Vitro Cytotoxicity Activities on Cancer Cell Lines. *J. Braz. Chem. Soc.* **2015**, *26*, 1838-1847.
- (63) Jia, G.; Rheingold, A. L.; Haggerty, B. S.; Meek, D. W. Synthesis and Characterization of Ruthenium Acetate Complexes Containing Triphosphines. *Inorg. Chem.* **1992**, *31*, 900-904.
- (64) Uznanski, P.; Zakrzewska, J.; Favier, F.; Kazmierski, S.; Bryszewska, E. Synthesis and Characterization of Silver Nanoparticles from (Bis)Alkylamine Silver Carboxylate Precursors. *J. Nanopart. Res.* **2017**, *19*, 121-121.
- (65) Toma, H. E.; Nikolaou, S. Self-Assembly of a Supramolecular Cyclic Polymer Containing Pyrazine Bridged Trinuclear M-Oxo-Ruthenium-Acetate Clusters. *J. Chem. Res.* **2000**, 326-327.
- (66) Toma, Henrique E.; Alexiou, Anamaria D. P.; Dovidauskas, S. Extended Electronic Interactions in a Triangular M-Oxotriruthenium Acetate Cluster Containing Nitric Oxide. *Eur. J. Inorg. Chem.* **2002**, 3010-3017.
- (67) Kepert, C. M.; Deacon, G. B.; Spiccia, L.; Fallon, G. D.; Skelton, B. W.; White, A. H. A Facile and Benign Synthesis of Binuclear Ruthenium(II) "Sawhorse" Complexes. *J. Chem. Soc., Dalton Trans.* **2000**, 2867-2873.
- (68) Wang, S.; Sim, W.-S. Au Nanoparticles Encapsulated in Ru Carbonyl Carboxylate Shells. *Langmuir* **2006**, *22*, 7861-7866.
- (69) Gibson, A. J.; Temperton, R. H.; Handrup, K.; Weston, M.; Mayor, L. C.; O'Shea, J. N. Charge Transfer from an Adsorbed Ruthenium-Based Photosensitizer through an Ultra-Thin Aluminium Oxide Layer and into a Metallic Substrate. *J. Chem. Phys.* **2014**, *140*, 234708.
- (70) Kellner, C. S.; Bell, A. T. Infrared Studies of Carbon Monoxide Hydrogenation over Alumina-Supported Ruthenium. *J. Catal.* **1981**, *71*, 296-307.
- (71) Dimakis, N.; Navarro, N. E.; Mion, T.; Smotkin, E. S. Carbon Monoxide Adsorption Coverage Study on Platinum and Ruthenium Surfaces. *J. Phys. Chem. C* **2014**, *118*, 11711-11722.
- (72) Pfnür, H.; Menzel, D.; Hoffmann, F. M.; Ortega, A.; Bradshaw, A. M. High Resolution Vibrational Spectroscopy of Co on Ru(001): The Importance of Lateral Interactions. *Surf. Sci.* **1980**, *93*, 431-452.
- (73) Starr, D. E.; Bluhm, H. Co Adsorption and Dissociation on Ru(0001) at Elevated Pressures. *Surf. Sci.* **2013**, *608*, 241-248.
- (74) Martínez-Prieto, L. M.; Urbaneja, C.; Palma, P.; Cámpora, J.; Philippot, K.; Chaudret, B. A Betaine Adduct of N-Heterocyclic Carbene and Carbodiimide, an Efficient Ligand to Produce Ultra-Small Ruthenium Nanoparticles. *Chem. Commun.* **2015**, *51*, 4647-4650.
- (75) González-Gálvez, D.; Nolis, P.; Philippot, K.; Chaudret, B.; van Leeuwen, P. W. N. M. Phosphine-Stabilized Ruthenium Nanoparticles: The Effect of the Nature of the Ligand in Catalysis. *ACS Catal.* **2012**, *2*, 317-321.
- (76) Chen, L.; Zhu, Y.; Zheng, H.; Zhang, C.; Zhang, B.; Li, Y. Aqueous-Phase Hydrodeoxygenation of Carboxylic Acids to Alcohols or Alkanes over Supported Ru Catalysts. *J. Mol. Cat. A* **2011**, *351*, 217-227.
- (77) Shangguan, J.; Olarte, M. V.; Chin, Y.-H. Mechanistic Insights on Co and Cc Bond Activation and Hydrogen Insertion During Acetic Acid Hydrogenation Catalyzed by Ruthenium Clusters in Aqueous Medium. *J. Catal.* **2016**, *340*, 107-121.
- (78) Cusinato, L.; Martínez-Prieto, L. M.; Chaudret, B.; del Rosal, I.; Poteau, R. Theoretical Characterization of the Surface Composition of Ruthenium Nanoparticles in Equilibrium with Syngas. *Nanoscale* **2016**, *8*, 10974-10992.
- (79) McCue, A. J.; Anderson, J. A. Recent Advances in Selective Acetylene Hydrogenation Using Palladium Containing Catalysts. *Front. Chem. Sci. Eng.* **2015**, *9*, 142-153.
- (80) López, T.; Hernandez-Ventura, J.; Asomoza, M.; Campero, A.; Gómez, R. Support Effect on Cu-Ru/SiO₂ Sol-Gel Catalysts. *Mater. Lett.* **1999**, *41*, 309-316.
- (81) Dhiman, M.; Chalke, B.; Polshettiwar, V. Efficient Synthesis of Monodisperse Metal (Rh, Ru, Pd) Nanoparticles Supported on Fibrous Nanosilica (Kcc-1) for Catalysis. *ACS Sustain. Chem. Eng.* **2015**, *3*, 3224-3230.
- (82) Li, C.; Shao, Z.; Pang, M.; Williams, C. T.; Zhang, X.; Liang, C. Carbon Nanotubes Supported Mono- and Bimetallic Pt and Ru Catalysts for Selective Hydrogenation of Phenylacetylene. *Ind. Eng. Chem. Res.* **2012**, *51*, 4934-4941.
- (83) Rakers, L.; Martínez-Prieto, L. M.; López-Vinasco, A. M.; Philippot, K.; van Leeuwen, P. W. N. M.; Chaudret, B.; Glorius, F. Ruthenium Nanoparticles Ligated by Cholesterol-Derived Nhcs and Their Application in the Hydrogenation of Arenes. *Chem. Commun.* **2018**, *54*, 7070-7073.
- (84) Ruzicka, J.-Y.; Anderson, D. P.; Gaw, S.; Golovko, V. B. Platinum-Ruthenium Nanoparticles: Active and Selective Catalysts for

- Hydrogenation of Phenylacetylene. *Aust. J. Chem.* **2012**, *65*, 1420-1425.
- (85) Niu, M.; Wang, Y.; Li, W.; Jiang, J.; Jin, Z. Highly Efficient and Recyclable Ruthenium Nanoparticle Catalyst for Semihydrogenation of Alkynes. *Catal. Commun.* **2013**, *38*, 77-81.
- (86) Noël, S.; Bourbiaux, D.; Tabary, N.; Ponchel, A.; Martel, B.; Monflier, E.; Léger, B. Acid-Tolerant Cyclodextrin-Based Ruthenium Nanoparticles for the Hydrogenation of Unsaturated Compounds in Water. *Catal. Sci. Technol.* **2017**, *7*, 5982-5992.
- (87) Maximov, A.; Zolotukhina, A.; Kulikov, L.; Kardasheva, Y.; Karakhanov, E. Ruthenium Catalysts Based on Mesoporous Aromatic Frameworks for the Hydrogenation of Arenes. *React. Kinet., Mech. Cat.* **2016**, *117*, 729-743.
- (88) Pechtl, M. H. G.; Scariot, M.; Scholten, J. D.; Machado, G.; Teixeira, S. R.; Dupont, J. Nanoscale Ru(o) Particles: Arene Hydrogenation Catalysts in Imidazolium Ionic Liquids. *Inorg. Chem.* **2008**, *47*, 8995-9001.
- (89) Nowicki, A.; Le Boulaire, V.; Roucoux, A. Nanoheterogeneous Catalytic Hydrogenation of Arenes: Evaluation of the Surfactant-Stabilized Aqueous Ruthenium(o) Colloidal Suspension. *Adv. Synth. Catal.* **2007**, *349*, 2326-2330.
- (90) Rossi, L. M.; Machado, G. Ruthenium Nanoparticles Prepared from Ruthenium Dioxide Precursor: Highly Active Catalyst for Hydrogenation of Arenes under Mild Conditions. *J. Mol. Cat. A* **2009**, *298*, 69-73.
- (91) Zahmakiran, M.; Özkar, S. Intrazeolite Ruthenium(o) Nanoclusters: A Superb Catalyst for the Hydrogenation of Benzene and the Hydrolysis of Sodium Borohydride. *Langmuir* **2008**, *24*, 7065-7067.
- (92) Salas, G.; Campbell, P. S.; Santini, C. C.; Philippot, K.; Costa Gomes, M. F.; Pádua, A. A. H. Ligand Effect on the Catalytic Activity of Ruthenium Nanoparticles in Ionic Liquids. *Dalton Trans.* **2012**, *41*, 13919-13926.
- (93) Tschan, M. J.-L.; Diebolt, O.; van Leeuwen, P. W. N. M. Ruthenium Metal Nanoparticles in Hydrogenation: Influence of Phosphorus-Ligands. *Top. Catal.* **2014**, *57*, 1054-1065.
- (94) Cui, X.; Surkus, A.-E.; Junge, K.; Topf, C.; Radnik, J.; Kreyenschulte, C.; Beller, M. Highly Selective Hydrogenation of Arenes Using Nanostructured Ruthenium Catalysts Modified with a Carbon-Nitrogen Matrix. *Nat. Commun.* **2016**, *7*, 11326-11326.
- (95) Gerber, I. C.; Serp, P. A Theory/Experience Description of Support Effects in Carbon-Supported Catalysts. *Chem. Rev.* **2019**, *120*, 1250-1349.
- (96) Susi, T.; Pichler, T.; Ayala, P. X-Ray Photoelectron Spectroscopy of Graphitic Carbon Nanomaterials Doped with Heteroatoms. *Beilstein J. Nanotechnol.* **2015**, *6*, 177-192.



Insert Table of Contents artwork here
